© 2019. Published by The Company of Biologists Ltd | Journal of Cell Science (2019) 132, jcs220624. doi:10.1242/jcs.220624

RESEARCH ARTICLE

Number and brightness analysis reveals that NCAM and FGF2 elicit different assembly and dynamics of FGFR1 in live cells

Moreno Zamai[1,2], Antonio Trullo[1,‡], Marco Giordano[3,‡], Valeria Corti[1], Elvira Arza Cuesta[2], Chiara Francavilla[4], Ugo Cavallaro[3,*,§] and Valeria R. Caiolfa[1,2,*,§]

ABSTRACT

Both fibroblast growth factor-2 (FGF2) and neural cell adhesion molecule (NCAM) trigger FGF receptor 1 (FGFR1) signaling; however, they induce remarkably distinct receptor trafficking and cellular responses. The molecular basis of such a dichotomy and the role of distinct types of ligand-receptor interaction remain elusive. Number of molecules and brightness (N&B) analysis revealed that FGF2 and NCAM promote different FGFR1 assembly and dynamics at the plasma membrane. NCAM stimulation elicits long-lasting cycles of short-lived FGFR1 monomers and multimers, a behavior that might reflect a rapid FGFR1 internalization and recycling. FGF2, instead, induces stable dimerization at the dose that stimulates cell proliferation. Reducing the occupancy of FGFR1 in response to low FGF2 doses causes a switch towards cyclically exposed and unstable receptor dimers, consistently with previously reported biphasic response to FGF2 and with the divergent signaling elicited by different ligand concentrations. Similar instability was observed upon altering the endocytic pathway. Thus, FGF2 and NCAM induce differential FGFR1 clustering at the cell surface, which might account for the distinct intracellular fate of the receptor and, hence, for the different signaling cascades and cellular responses.

KEY WORDS: Receptor clustering, FGF, FGFR1, NCAM, N&B analysis, FGFR1 signaling, FGFR1 clustering

INTRODUCTION

Fibroblast growth factor receptors (FGFRs) form a highly conserved receptor tyrosine kinase (RTK) subfamily (FGFR1, FGFR2, FGFR3 and FGFR4) that regulates essential cellular processes, including proliferation, survival, migration and differentiation during development and adult life. The deregulation of FGFR activity plays a pathogenic role in various diseases, which include skeletal and metabolic disorders. In addition, uncontrolled FGFR signaling has been implicated in several tumor types and represents a viable target for anticancer treatments (Babina and Turner, 2017).

FGFRs signaling is initiated by the binding of canonical growth factors, the FGFs, that induces FGFR dimerization and autophosphorylation of up to seven tyrosine residues in the intracellular catalytic domain (Beenken and Mohammadi, 2009). The stimulation of the receptors generates multiple docking sites for several adaptor and effector proteins (Eswarakumar et al., 2005), resulting in the activation of various downstream signaling cascades that have been extensively described (Belov and Mohammadi, 2013; Furdui et al., 2006)

FGFRs can also be activated by cell adhesion molecules, including neural cell adhesion molecule (NCAM) (Hansen et al., 2008; Sanchez-Heras et al., 2006; Williams et al., 1994). The latter belongs to the immunoglobulin (Ig) superfamily and has a structure consisting of five Ig-like and two fibronectin type III extracellular modules and a cytoplasmic part of variable length. The direct binding of NCAM to FGFR1 has been demonstrated in cell-free systems (Kiselyov et al., 2003) and in several cell types (Cavallaro et al., 2001; Francavilla et al., 2007; Kos and Chin, 2002; Sanchez-Heras et al., 2006). We have previously reported that the interaction between NCAM and FGFR1 enhances tumor progression and represents a therapeutic target (Zecchini et al., 2011), thus underscoring its biological and clinical relevance in molecular oncology.

NCAM, on one hand, inhibits the binding of FGF to its receptor (Francavilla et al., 2007) and, on the other hand, acts itself as a nonconventional ligand for FGFR1, as supported by the evidence of direct physical interaction between the two molecules (Christensen et al., 2006; Francavilla et al., 2009; Kiselyov et al., 2003; Kos and Chin, 2002). The ectodomain of NCAM and fragments thereof can be released from the cell surface, implying the possibility that they act as soluble FGFR ligands. Accordingly, soluble NCAM-Fc and the NCAM-derived dendrimeric peptide FGL have been employed to trigger FGFR activation (Francavilla et al., 2009; Kiselyov et al., 2003). In particular, we have shown that NCAM-Fc-mediated activation of FGFR1 elicits a cellular response distinct from that stimulated by FGF2. As for most RTKs, canonical ligand binding induces the formation of a dimeric $FGFR_2$–$ligand_2$ complex that internalizes and undergoes Cbl-mediated ubiquitylation followed by lysosomal degradation (Wong et al., 2002). In contrast to degradation of endocytic FGFR1, soluble NCAM-Fc promotes the recycling of the receptor to the cell surface in a Rab11- and Src-dependent manner (Francavilla et al., 2009). We have also demonstrated that soluble NCAM-Fc induces a specific set of FGFR1-dependent biochemical events that i) require recycling of the receptor, ii) occur in the absence of cell surface NCAM, iii) result in sustained signaling and iv) lead to cell migration (Francavilla et al., 2009). Importantly, soluble NCAM-Fc and the FGL peptide fully recapitulate the physiological activities of membrane-associated NCAM (Cavallaro et al., 2001; Christensen et al., 2006; Francavilla et al., 2009; Kiselyov et al., 2003; Thomaidou et al., 2001), inducing FGFR1-dependent matrix adhesion in different cell types (Cavallaro et al., 2001; Francavilla et al., 2009), promoting

[1]Centro di Imaging Sperimentale (CIS), Ospedale San Raffaele, IRCCS, Milan 20132, Italy. [2]Microscopy and Dynamic Imaging Unit, Centro Nacional de Investigaciones Cardiovasculares (CNIC), Madrid 28029, Spain. [3]Unit of Gynecological Oncology Research, European Institute of Oncology IRCCS, Milan 20141, Italy. [4]Division of Molecular and Cellular Functions, School of Biological Sciences, Faculty of Biology, Medicine and Health, University of Manchester, Manchester M13 9PL, UK.
*These authors contributed equally to the work
‡These authors contributed equally to the work

§Authors for correspondence (valeria.caiolfa@hsr.it, ugo.cavallaro@ieo.it)

V.R.C., 0000-0003-4814-6490

Received 22 May 2018; Accepted 15 November 2018

Journal of Cell Science (2019) 132, jcs220624. doi:10.1242/jcs.220624

neurite outgrowth (Kiselyov et al., 2003), and exerting a pro-migratory activity during epithelial–mesenchymal transition (Lehembre et al., 2008).

Up to date, the molecular basis of the dichotomy between NCAM and FGF-induced FGFR1 signaling is unclear. The different affinity for FGFR1 between FGF and NCAM-derived ligands (Kiselyov et al., 2003) could imply the formation of distinct stoichiometric complexes on the cell membrane. These, in turn, would elicit different internalization pathways and signaling mechanisms.

We tested this hypothesis by exploring the spatio-temporal dynamics of FGFR1 molecules at the cell membrane following the activation with either FGF2 or the NCAM-derived ligands NCAM-Fc and FGL. Our approach relied on the number of molecules and brightness (N&B) technique, a pixel-by-pixel moment-analysis that allows to investigate protein association and clustering in different biological contexts (Digman et al., 2008; Hellriegel et al., 2011; Nagy et al., 2010; Olivera-Couto et al., 2015; Perumal et al., 2015; Plotegher et al., 2014; Trullo et al., 2013). Our data show, for the first time, that – in contrast to FGF2-induced dimerization of FGFR1 – NCAM triggers the formation of unstable FGFR1 homomultimers. Furthermore, NCAM-induced FGFR1 complexes cycle rapidly and repeatedly at the cell surface. Of note, such dynamics of the FGFR1 complexes were also observed in FGF2-stimulated cells upon interference with internalization and the intracellular degradation of the $FGFR1_2$–$FGF2_2$ complex or by using low concentrations of FGF2.

Our study, therefore, highlights a dichotomy in the assembly of FGFR1 upon stimulation with NCAM or FGF2 that may contribute to explain the divergent responses of the receptor to the two ligands.

RESULTS

NCAM and FGF2 induce the formation of FGFR1 complexes with different molecular organization and kinetics

For N&B analysis, we forced the ectopic expression of FGFR1 fused at the C-terminus to monomeric EGFP (mEGFP) (Fig. 1A) in HeLa cells. This cell line has negligible levels of endogenous FGFR1 (Fig. 1B). Thus, the brightness measured can be ascribed to ligand-induced oligomerization of FGFR1-mEGFP, assuming no contribution from endogenous, unlabeled receptor molecules. In addition, we have selected mEGFP as the fluorophore because, unlike wild-type EGFP, it does not self-aggregate (Caiolfa et al., 2007) thus reducing the risk of GFP-induced clustering of the tagged receptor. FGFR1-mEGFP transiently transfected in HeLa cells localized abundantly on the plasma membrane and was also present in the Golgi and intracellular vesicular structures (Fig. 1C and Fig. S1). Moreover, FGF2 stimulation induced a 15-fold increase in FGFR1 phosphorylation (Fig. 1D). The low amount of constitutively activated FGFR1 detected in unstimulated cells was likely due to the high overexpression of FGFR1-mEGFP in a small fraction of cells (not shown). We also verified that FGF2 treatment promoted the activation of classical FGFR1 effectors such as FRS2a and Erk1/2 (data not shown). Overall, these observations indicate

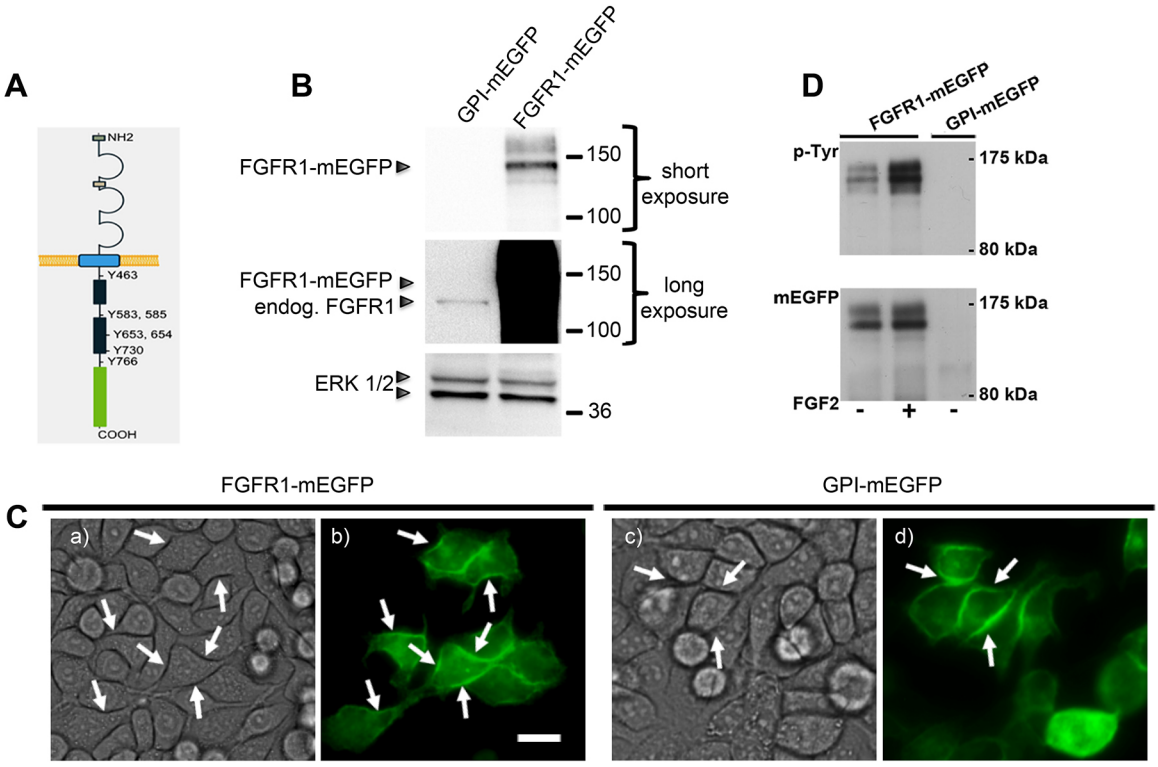

Fig. 1. Functional FGFR1-mEGFP fusion protein in HeLa cells. (A) Schematic representation of FGFR1 fused with C-terminal mEGFP (green box). The tyrosine (Y) autophosphorylation sites in the cytoplasmic tail are shown. (B) FGFR1 immunoblotting analysis in HeLa cells transiently transfected either with GPI-mEGFP (left lane) or FGFR1-mEGFP (right lane). A blot with long exposure time is shown to reveal the very low levels of endogenous FGFR1 (middle panel). Immunoblotting for ERK 1/2 served as loading control (lower panel). (C) Representative bright field (a, c) and epifluorescence images (b, d) of live HeLa cells transiently transfected with FGFR1-mEGFP (a, b) or GPI-mEGFP (c, d). Arrows indicate membrane localization. Scale bar: 20 µm. No fluorescence signal was detected in non-transfected cells. (D) FGFR1-mEGFP activation by FGF2. HeLa cells transfected with either FGFR1-mEGFP or GPI-mEGFP were serum-starved overnight and then left untreated or stimulated for 10 min with 20 ng/ml FGF2. Lysates were immunoprecipitated with an anti-FGFR1 antibody, followed by immunoblotting for phosphotyrosine (p-Tyr; upper panel) or GFP-tagged mEGFP (mEGFP, lower panel).

Journal of Cell Science (2019) 132, jcs220624. doi:10.1242/jcs.220624

that FGFR1-mEGFP recapitulates the subcellular distribution and the biochemical functionality of wild-type FGFR1.

The brightness of membrane-associated FGFR1-mEGFP was measured by imaging the cells by total internal fluorescence reflection (TIRF) microscopy. Based on the intrinsic features of evanescent illumination, the TIRF image depicts the ventral side of the plasma membrane without interference coming from intracellular fluorescence signals (Fig. S1C) (Poulter et al., 2015). The brightness of the monomeric and dimeric mEGFP tags was calibrated using two control constructs encoding glycosylphosphatidylinositol (GPI)-anchored mEGFP and mEGFP-mEGFP, that served as reliable standards in previous studies on cell surface receptors (Hellriegel et al., 2011). As shown in Fig. 2, which illustrates the calibration assay, the average brightness of GPI-mEGFP-mEGFP from replicate experiments $\langle\varepsilon\rangle_{dimer}$=0.205±0.006 ((counts/molecule)×dwell time) was reproducibly equal to the double of the GPI-mEGFP brightness $\langle\varepsilon\rangle_{monomer}$=0.103±0.004 ((counts/molecule)×dwell time) (P<0.0001). Of note, we did not detect fluorescent clusters, confirming the lack of spontaneous clustering of ectopic mEGFP at the cell membrane.

To determine the effects of the different stimuli on FGFR1 clustering, HeLa cells expressing FGFR1-mEGFP were treated with either FGF2 or NCAM-derived ligands. We used concentrations known to induce FGFR1 autophosphorylation and activation, thus eliciting signaling cascades and cell proliferation or migration (Francavilla et al., 2009). In unstimulated cells, the average brightness of FGFR1-mEGFP averaged over the entire image (Fig. 3A,C; B-maps at t=0) was equivalent to the brightness of GPI-mEGFP (B-map in Fig. 2A, top panel), indicating the predominance of monomeric receptors. After FGF2 addition, the average brightness increased sharply during the first 5-15 min (B-maps in Fig. 3A, top panel), reaching a plateau at values similar to those measured in GPI-mEGFP-mEGFP cells (B-map in Fig. 2A, bottom panel), thus indicating the formation of FGFR1-mEGFP homodimers. The average brightness dynamics of FGFR1-mEGFP as a function of time from replicate experiments is summarized in Fig. 3B. Between 5 and 15 min after ligand stimulation, the average brightness increased sharply up to two-fold the baseline value, consistent with the recruitment and dimerization of FGFR1-mEGFP molecules at the cell membrane, and remained at plateau for ∼10 min (Fig. 3B). The average fluorescence intensity of the imaged cells varied from one to another (not shown), yet the maximum of intensity was reproducibly reached in the same interval of time (5–15 min of stimulation). Overall, these results demonstrated the formation of stable receptor homodimers at the cell membrane. Of note, the heteroassociation of FGFR1 with other FGFR family members has never been reported. Thus, N&B analysis reflected the dimerization of FGFR1 induced by its canonical ligand in our cellular model. In addition, the negligible levels of endogenous FGFR1 in HeLa cells (Fig. 1B) ruled out the formation of larger complexes containing non-fluorescent, endogenous FGFR1. In summary, our results indicated the predominance of monomeric FGFR1-mEGFP at the cell membrane of unstimulated HeLa cells, and its sustained dimerization upon activation with 20 ng/ml FGF2. We also monitored the localization of endogenous FGFR1 by immunofluorescence and confocal microscopy in the OVCAR3 cell line upon FGF2 stimulation. FGFR1 was expressed at the cell surface in unstimulated cells and, to a greater extent, after a 10-min incubation with FGF2, while at longer time points we observed intracellular accumulation and decreased immunoreactivity (Fig. S2), suggestive of internalization and degradation. Similar results were obtained with the cell line OV90 (not shown).

As exemplified in Fig. 3C, the self-association of FGFR1-mEGFP stimulated with NCAM-Fc was dramatically different from that induced by FGF2. Indeed, we observed fast and cyclic transitions of the average brightness that rose from the basal value, corresponding to monomeric state, to three-fold higher values (Fig. 3C–B-maps and Frequency Histograms). Such association/dissociation cycles of FGFR1-mEGFP persisted for over an hour

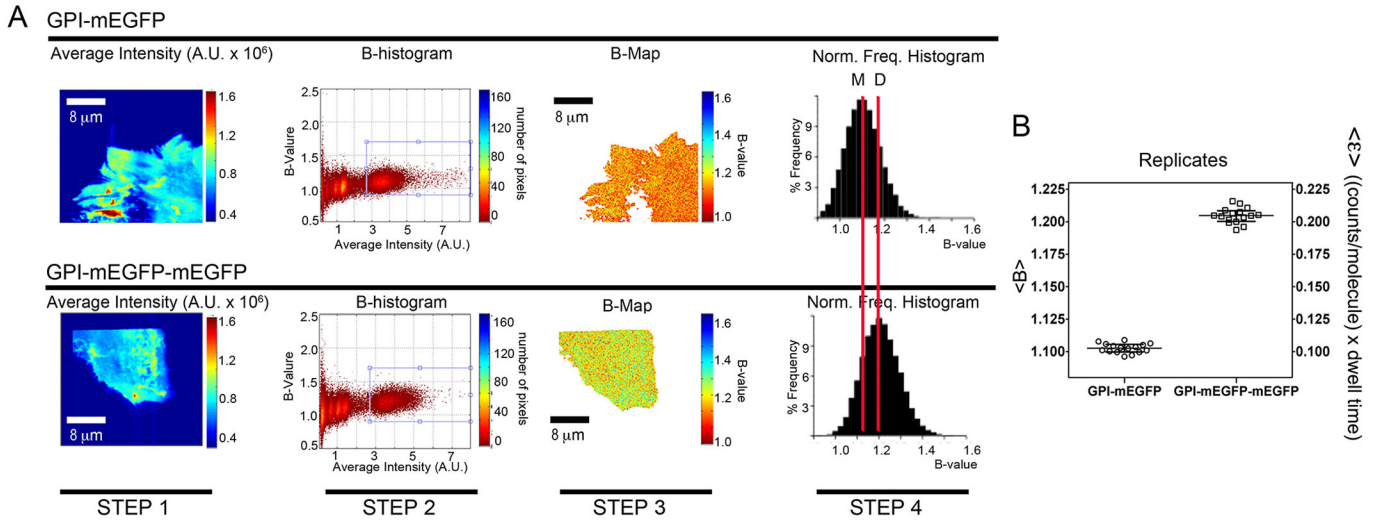

Fig. 2. Brightness calibration by GPI-mEGFP and GPI-mEGFP-mEGFP control constructs expressed in HeLa cells. The experimental procedure (STEP 1–4) is shown for two representative HeLa cells expressing the monomeric GPI-mEGFP (top) or the dimeric GPI-mEGFP-mEGFP (bottom) control constructs. For each control construct, the average intensity is obtained from a time series acquired on a single cell according to (Digman 2008) and Eqn 1 (STEP1), and processed in the B-histogram according to Eqn 2 (STEP 2). The blue rectangle in the B-histograms shows the region of interest (ROI) that was chosen to construct the B-maps (STEP3) and normalized frequency histograms (Norm. Freq. Histogram; STEP4) above the background threshold; in the latter red lines mark the central values for the two representative examples of the monomer (M) and the dimer (D) distribution. (B) Plot of the averaged B-values (<B>) as obtained in A from three independent experiments performed for each control construct (5–7 cells/experiment). Data are provided as average B-value/cell (left y-axis) and as <ε> in [(counts/molecule) x dwell time] (right y-axis) according to Eqn 2. <ε> proportionally increases with the increase of mEGFP molecules in the control constructs: $\langle\varepsilon\rangle_{monomer}$=0.103±0.004 s.d. and $\langle\varepsilon\rangle_{dimer}$=0.205±0.006 s.d. [(counts/molecule) x dwell time]; (P<0.0001).

Journal of Cell Science (2019) 132, jcs220624. doi:10.1242/jcs.220624

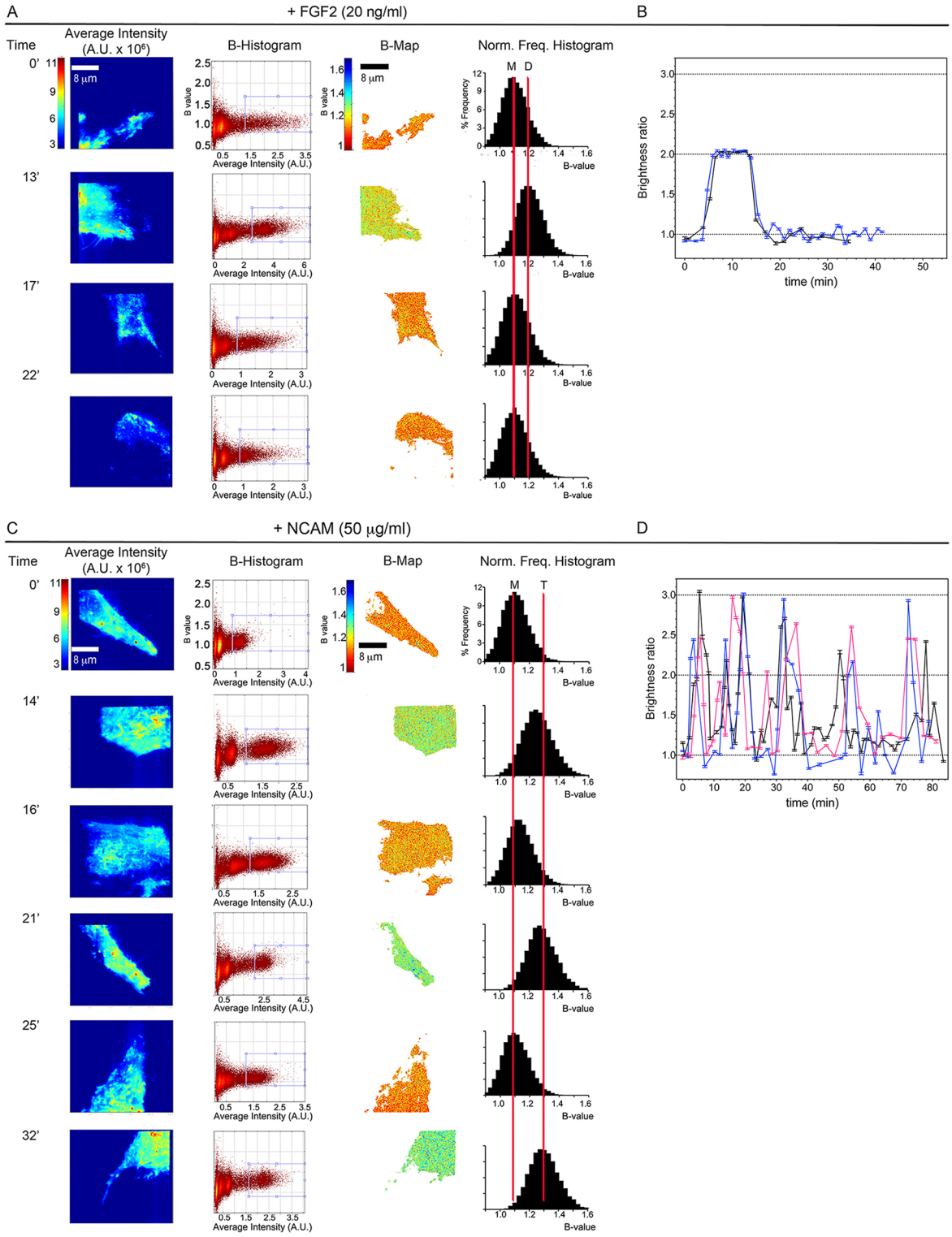

Fig. 3. Ligand-induced time-dependent assembly of FGFR1-mEGFP expressed in HeLa cells. Representative examples of time-dependent brightness of FGFR1-mEGFP expressed in HeLa cell upon treatment with 20 ng/ml FGF2 (A) or 50 µg/ml NCAM-Fc (C). TIRF sequences were acquired at 0, 13, 17 and 22 minutes after FGF2 stimulation (A) and at 0, 14, 16, 21, 25, and 32 minutes after NCAM stimulation (C). For each time point, the N&B analysis was performed starting from the average intensity (1st column) as described for Fig. 2 and in Materials and Methods. The blue rectangle in the B-histograms (2nd column) shows the region of interest (ROI) that was chosen to construct the B-maps (3rd column) and normalized frequency histograms (Norm. Freq. Histogram; 4th column) above the background threshold; in the latter red lines mark the B-central values (average brightness) associated to mEGFP monomers (M), mEGFP dimers (D) and putative mEGFP trimers (T) distribution, as an indication of the shift observed during the kinetic runs. (B,D) Plots of normalized average brightness as a function of time. Each value was obtained from the analysis of at least 6000 pixels/image x time point as $<\varepsilon>= B-1$ (Eqn. 2), normalized to the basal value at t=0 min, before ligand addition and reported as brightness ratio according to Eqn 3. Data (±s.e.m.) in panels B and D refer to two and three independent kinetic runs, with 37 (blue line) and 19 (black line) cells in (B), and 64 (black line), 40 (blue line) and 43 (red line) cells in D. Scales and axis labels are shown at time = 0 in A and C and apply to all time points of each kinetic run.

Journal of Cell Science (2019) 132, jcs220624. doi:10.1242/jcs.220624

after NCAM-Fc stimulation (Fig. 3D). Moreover, as illustrated in Fig. 3D, the receptors transited through diverse and unstable multimeric mixtures that did not form upon stimulation with FGF2.

To confirm and extend the observations on NCAM-stimulated FGFR1, HeLa cells expressing FGFR1-mEGFP were also stimulated with the NCAM-derived peptide FGL, which recapitulates the binding to and the activation of FGFR1 (Francavilla et al., 2009; Kiselyov et al., 2003). We recorded brightness kinetics substantially similar to that observed in the presence of NCAM-Fc, with FGFR1-mEGFP state transitions of comparable magnitude and persistence (Fig. S3), and in both cases we never observed a normalized <ε> value above 3. Thus, in contrast to FGF2, neither NCAM-Fc nor the FGL peptide induced stable dimerization of FGFR1. Rather, both NCAM-derived ligands promoted the formation of unstable and heterogeneous FGFR1 multimers. It is noteworthy that, although a different cell was imaged at each time point for a total of 40–60 cells analyzed in each experiment, the average brightness never went above three times that of the monomeric receptor. This raised the intriguing hypothesis that NCAM-derived ligands induce a population of receptor trimers that predominate on the cell surface in a transient and cyclic fashion. In order to test the trimerization hypothesis biochemically, we attempted to crosslink the complexes between FGFR1-mEGFP and ligand (FGFR1-mEGFP–ligand). Upon cell stimulation with FGF2 and crosslinking, we could promptly detect dimeric FGFR1-mEGFP (Fig. S4). However, we did not succeed in detecting species larger than the monomer when cells were treated with NCAM-Fc or FGL, possibly due to the very transient nature of NCAM-induced FGFR1-mEGFP complexes on the cell membrane.

Taken together, these results demonstrate for the first time that, in contrast to the well-established receptor dimerization induced by FGF2, the non-canonical soluble NCAM ligands elicit transient and cyclic multimerization of FGFR1. While the N&B data would be consistent with the hypothesis of NCAM-induced trimerization of the receptor, this remains to be formally proven.

Low FGF2 concentrations mimic the NCAM-induced cyclic dynamics but do not alter the dimeric stoichiometry of FGFR1 complexes

The cyclic behavior and the instability of the NCAM–FGFR1 complexes might depend on the non-saturated binding sites due to the low affinity of NCAM-derived ligands as opposed to the high affinity of FGF2. If this were the case, it is conceivable that low concentrations of FGF2, being unable to saturate the ligand-binding sites in FGFR1-mEGFP-transfected cells, produce a similar instability. Thus, we determined the average brightness obtained in cells treated with decreasing concentrations of FGF2. At 10 ng/ml, FGF2 evoked a relatively stable dimerization of the receptor (Fig. 4A), with a very similar pattern to that observed with the full dose of 20 ng/ml (see Fig. 3B). However, when the FGF2 concentration was decreased to 2 ng/ml, the average brightness kinetics changed radically and showed cyclic transitions similar to those induced by NCAM-Fc (Fig. 4B). The concentration of the receptors exposed at the cell surface did not change significantly with time since the average fluorescence intensity was stable during the entire assay. Dimers were generated, as indicated by the average brightness ratio approaching a value of 2, but they did not reached a stable plateau as those induced by higher FGF2 doses. At such a low concentration as 1 ng/ml, the rate of FGF2-induced dimerization of FGFR1 was quite inefficient. Indeed, we observed the formation of mixtures of dimers and monomers yielding always an average brightness ratio of a value below 2 and a persistent surface exposure of the receptors (Fig. 4C).

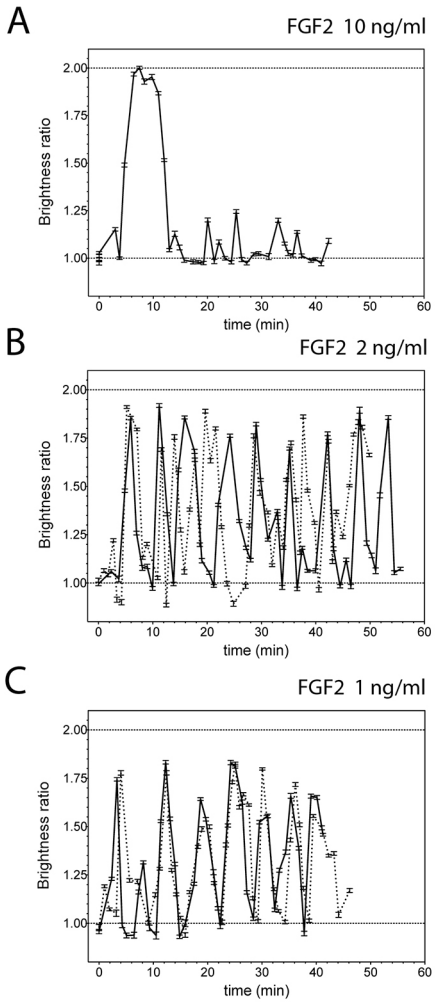

Fig. 4. Assembly and dynamics of the FGFR1 complexes are dependent on FGF2 concentration. (A,B) FGFR1-mEGFP-transfected HeLa cells were stimulated with FGF2 at 10 ng/ml (A), 2 ng/ml (B) or 1 ng/ml (C), followed by measurement of brightness as a function of time. Data (±s.e.m.) were obtained as described for Fig. 3 and refer to independent kinetic runs. Analyzed were 38 cells in A; 50 (dotted lines) and 46 (solid lines) cells in B; 46 (dotted lines) and 38 (solid lines) cells in C.

Taken together, these findings support the hypothesis that non-saturating concentrations of FGF2 result in unstable FGFR1–ligand complexes, thus recapitulating the cyclic pattern of mixed receptor complex species induced by NCAM-derived ligands. However, in striking contrast to NCAM, the highest average brightness induced by FGF2 was never above the value corresponding to dimers. This implies that the stoichiometry of FGFR1 complexes is ligand-specific.

The kinetics of FGFR1–FGF2 complexes at the cell surface is regulated by receptor ubiquitylation but not recycling

Following the binding of FGF2, FGFR1 signaling is attenuated by receptor internalization and Cbl-mediated ubiquitylation, which targets it to lysosomal degradation (Wong et al., 2002). We hypothesized that the intracellular fate of FGFR1 influences the dynamics and the stoichiometry of receptor complexes at the cell surface. To test this hypothesis, the endocytic pathway of FGFR1-mEGFP in HeLa cells was manipulated through the ectopic expression of either a dominant-negative variant or the wild-type form of Cbl (Germano et al., 2006). Indeed, we have previously

Journal of Cell Science (2019) 132, jcs220624. doi:10.1242/jcs.220624

shown that dominant-negative Cbl impairs FGF2-induced internalization and degradation of FGFR1, leading instead to receptor recycling (Francavilla et al., 2009). Thus, we stimulated HeLa cells expressing dominant-negative Cbl with 20 ng/ml FGF2, i.e. the dose that induces the formation of stable FGFR1 dimers. As shown in Fig. 5A (top panel), preventing Cbl-mediated ubiquitylation of FGFR1 affected dramatically its response to FGF2. In particular, the receptor dimers were highly unstable, and the average brightness ratio showed long-lasting transitions between predominantly dimeric and monomeric states, with the presence of intermediate mixtures of the two receptor species. This cyclic behavior started ∼10 min after the ligand addition, with a marked delay when compared to the receptor dimerization starting at ∼5 min in parental HeLa cells (see Fig. 3B). The expression of wild-type Cbl, instead, resulted in rapid and stable dimerization of FGFR1-mEGFP, followed by the decline to the initial monomeric baseline (Fig. 5A, bottom panel), thus recapitulating the response elicited by 20 ng/ml FGF2 in parental cells. These findings indicated that an intact Cbl-dependent endocytic pathway is required for the formation and persistence of FGFR1 dimers at the cell surface upon FGF2 stimulation, while perturbing the pathway destabilizes the dimers and triggers rapid and cyclic monomer/dimer transitions.

Several lines of evidence implicate membrane microdomains, such as lipid rafts and caveolae, in FGFR activity and trafficking (Asimaki et al., 2011; Fecchi et al., 2012; Gleizes et al., 1996; Irschick et al., 2013; Ridyard and Robbins, 2003; Wiedlocha and Sorensen, 2004). To investigate whether such microdomains are also involved in the assembly of FGFR1 complexes, HeLa cells expressing FGFR1-mEGFP were pre-treated with filipin, a drug that depletes cholesterol, and disrupts lipid rafts and caveolae (Lajoie and Nabi, 2007) prior to FGF2 stimulation. As illustrated in Fig. 5B, filipin pre-treatment evoked a response to FGF2 that is highly reminiscent of that observed with dominant-negative Cbl, with destabilization of functional FGFR1 dimers and repeated transitions between monomeric, dimeric and intermediate states. Thus, lipid rafts and/or caveolae microdomains play an important role in the dynamics and stoichiometry of FGFR1 complexes in response to FGF2.

We have previously reported that NCAM-derived ligands, but not FGF2, promote recycling of FGFR1 following internalization (Francavilla et al., 2009). Consistent with that observation, the inhibition of receptor recycling with the drug monensin (Basu et al., 1981; Felder et al., 1990) did not significantly alter the brightness kinetics of the FGFR1-mEGFP stimulated with 20 ng/ml FGF2. Indeed, dimers represented the predominant receptor species at the cell surface for ∼10 min (Fig. S5A). Rather, monensin affected the response to NCAM-Fc stimulation (Fig. S5B). In this case, the receptor complex with a brightness ratio of three times the monomeric value was detected only in one short cycle of ∼2–3 min after stimulation. In the subsequent cycles, the average brightness was at best twice the monomer baseline. Thus, the N&B analysis confirmed and extended our previous observations on the key role of FGFR1 recycling in the specific response of the receptor to NCAM-induced stimulation (Francavilla et al., 2009).

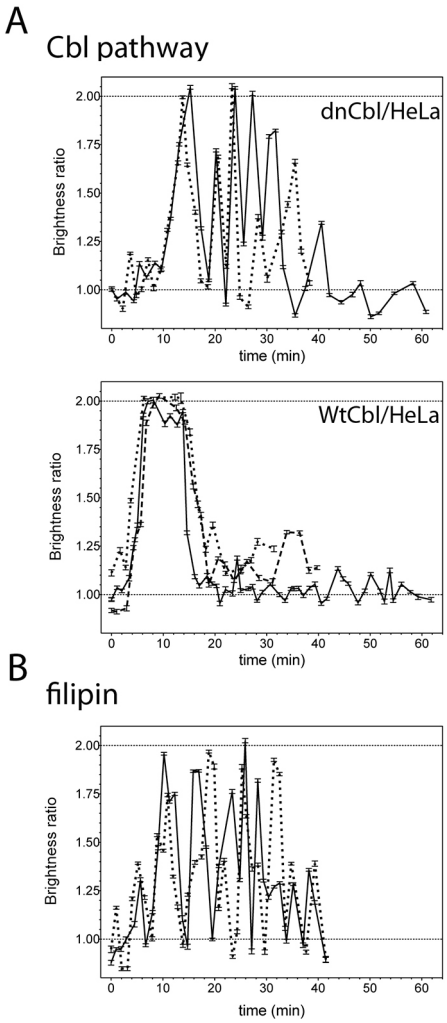

Fig. 5. The endocytic pathway influences the assembly of FGFR1 complexes. FGFR1-mEGFP was expressed in dominant-negative Cbl-Hela (dnCbl; A top panel), wild-type Cbl-Hela (WtCbl; A bottom panel) or in wild-type Hela cells pre-treated with 5 µg/ml filipin for 30 minutes (B). After stimulation with 20 ng/ml FGF2, the brightness as a function of time was obtained and normalized to the basal value, as described for Fig. 3, to follow the stoichiometric changes of FGFR1 clusters in A,B. Data (±s.e.m) were obtained as described for Fig. 3 and refer to independent kinetic runs. Analyzed were: 34 (solid line) and 27 (dotted line) cells in A (top); 24 (dashed line), 54 (solid line) and 16 (dotted line) cells in A (bottom); 34 (solid line) and 35 (dotted line) cells in B.

DISCUSSION

NCAM acts as a non-canonical ligand for FGFR1 and induces an FGFR1-mediated cellular response that is remarkably distinct from that elicited by FGF2 (Francavilla et al., 2009). However, the molecular basis of such a dichotomy and the role of distinct types of ligand-receptor interaction remain elusive. To address these issues, we applied the N&B analysis to time-lapse TIRF imaging and revealed that FGF2 and NCAM induce distinct assembly and dynamics of FGFR1 molecules at the surface of HeLa cells.

On the basis of our previous work (Francavilla et al., 2009) and in order to perform a direct comparison with exogenously added FGF2, we have used soluble NCAM-derived ligands, i.e. NCAM-Fc, the ectodomain of NCAM that occurs as a dimer because of the spontaneous Fc dimerization, and the NCAM-derived peptide FGL, which has a dendrimeric configuration with four peptides attached to a three-lysine backbone (Kiselyov et al., 2003). In contrast with the FGFR1 stable dimers induced by FGF2, the stimulation with NCAM-Fc or FGL resulted in apparently unstable and heterogeneous homoassociation of the FGFR1 molecules. It should be noticed that, due to photobleaching and photodamaging caused by repeated illumination, N&B analysis is intrinsically incompatible with imaging the same cell for prolonged time intervals. Therefore, the

Journal of Cell Science (2019) 132, jcs220624. doi:10.1242/jcs.220624

stable or unstable nature of FGFR1-mEGFP complexes in FGF2 or NCAM-stimulated cells, respectively, can only be deduced from the average brightness values that are recorded in the different cells imaged at different time points and, therefore, remains to be formally proven. We observed long-lasting cycles during which the receptor shifted from the monomeric form to a state or a mixture of states consistent with an average brightness of three monomeric units, with intermediate combinations occurring between the two predominant conditions. The N&B analysis could not find regions of the cell membrane associated to an average brightness larger than three monomeric FGFR1 units. Additionally, our biochemical approach (crosslinking and immunoblotting) failed to detect FGFR1-mEGFP trimers in cells that were exposed to NCAM-derived ligands. A likely explanation for this is the very transient nature of NCAM-induced FGFR1-mEGFP complexes on the cell membrane, as indicated by the N&B analysis (see Fig. 3D and Fig. S1B). We have previously reported that, upon NCAM stimulation, FGFR1 undergoes rapid endocytosis and recycling at the cell surface (Francavilla et al., 2009). On the basis of those findings, one can speculate that the fast transitions of NCAM-stimulated FGFR1 into different stoichiometric states reflect rapid internalization and recycling of receptor molecules assembled in heterogeneous and unstable multimers that cannot be captured and visualized in end-point batch biochemical analysis. Obviously, our inability to detect FGFR1 trimers biochemically might also depend on other factors, either technical or biological. In this context, we cannot resolve the cluster composition associated to the average brightness of 3-fold the monomeric unit. Thus, the possibility remains that the average brightness of 3-fold the monomer value reflects random mixtures of large FGFR1-mEGFP oligomers and monomers. Nevertheless, not only did we systematically and reproducibly measure an average brightness corresponding to a trimer, but the pattern was quantitatively and qualitatively similar with both NCAM-Fc and the FGL peptide. In this context, although our study provides the first observation of trimerization of a growth factor receptor, other types of receptor have been reported to form biologically active trimers at the cell surface, including members of the tumor necrosis factor receptor (TNFR) and of the plexin families (Anastasia et al., 2015; Balasubramanian and Zhang, 2015; Sedger and McDermott, 2014). Incidentally, TNFR trimers appear to be only transiently expressed on the cell surface (Sedger and McDermott, 2014), which combined with our data on NCAM-induced FGFR1 complexes, implies that a trimeric conformation of cell-surface receptors might confer instability.

The instability of NCAM–FGFR1 complexes might depend on the ligand affinity. Indeed, the low (micromolar) affinity of soluble NCAM ligands for FGFR1 (Kiselyov et al., 2003), as compared with the high (picomolar) affinity of FGF2 (Mohammadi et al., 2005), might result in binding sites not being saturated. This would make the NCAM-receptor complexes unstable. In support of this hypothesis, the decrease in the concentration of FGF2 also resulted in unstable and cyclic FGFR1 homoassociation, thus mimicking to some extent the effect of NCAM stimulation.

To gain insights into the stoichiometry of the FGFR1 complexes upon NCAM-mediated stimulation, other approaches, such as single-point photon-counting histograms (Chen et al., 2002) or cumulant analysis (M; ler, 2004), could resolve heterogeneous receptor populations better than N&B. Yet, these approaches require a large number of observations at each pixel, are computationally slow and not applicable to the analysis of all pixels in an image (Digman and Gratton, 2011). Additional methods with the capability of resolving mixtures, such as stepwise photobleaching (Coffman and Wu, 2012), cannot be applied to fast dynamics in live cells. Rather, recent studies based on N&B analysis (Digman et al., 2008; Hellriegel et al., 2011; Nagy et al., 2010; Olivera-Couto et al., 2015; Perumal et al., 2015; Plotegher et al., 2014; Trullo et al., 2013), and our present results point to this approach as a valuable tool to study the fast and dynamic organization of cell surface molecules, thus complementing and extending the information provided by other imaging and biochemical approaches. In light of these considerations, the interpretation of our N&B data should take into account that the individual species of FGFR1-mEGFP in multimeric mixtures cannot be resolved under our experimental conditions. Hence, the stoichiometry of FGFR1 complexes upon NCAM stimulation, although clearly different than that induced by FGF2, remains an open question.

Our previous work has revealed that, unlike FGF2, NCAM induces the recycling of FGFR1 at the cell surface which, in turn, accounts for NCAM-induced sustained signaling and cell migration, as opposed to the transient activation of FGFR1 and the proliferative effect induced by FGF2 (Francavilla et al., 2009). In light of the results presented here, it is possible that the different clustering and dynamics of the receptor complexes elicited by NCAM and FGF2 contribute to the previously reported dichotomy in the response of FGFR1 to the two ligands (Francavilla et al., 2009). It is conceivable, indeed, that the ligand-specific modes of FGFR1 assembly determine different internalization mechanisms, different intracellular fate of the FGFR1–ligand complexes and, hence, distinct signaling cascades.

The investigation of the internalization mechanisms is beyond the scope of this work, yet we have explored the assembling dynamics of the receptor at low FGF2 concentrations, asking whether the reduction of the occupancy of FGFR1 by its classic ligand causes a switch towards unconventional FGFR1 dynamics, such as that induced by NCAM. Previous reports have described a biphasic response to FGF2 stimulation in cell models. *In vitro* studies showed that the intracellular effectors, the signaling duration and the cellular response are strictly dependent on the concentration of FGF2 (in a range between 0.01 and 100 ng/ml), with different FGF2 doses evoking opposite responses (Garcia-Maya et al., 2006). By using a combined approach of computational modeling and experiments, Kanodia and colleagues found that the competition of FGF2 binding to either cell surface heparan sulfate glycosaminoglycans (HSGAGs) or FGF receptor leads to the biphasic response observed in several *in vitro* systems (Kanodia et al., 2014). In our cell model, at low FGF2 doses the N&B analysis shows that stability of the membrane-exposed FGFR1 dimers is reduced, resulting in a fast and cyclic dynamics of monomers and dimers with predominance of intermediate mixtures. Thus, we provide the first spatio-temporal visualization of the FGFR1 engagement by FGF2, which is consistent with and complements previous observations that have highlighted the influence of ligand gradients in fundamental processes, such as cell proliferation, survival and differentiation (Garcia-Maya et al., 2006).

We have previously shown that Cbl inactivation results in FGFR1 recycling to the cell surface – even upon stimulation with 20 ng/ml FGF2 – as opposed to the receptor internalization and degradation observed in Cbl-proficient cells. As a consequence, FGF2 becomes able to elicit a receptor response that is very similar to that of NCAM, with sustained signaling and cell migration (Francavilla et al., 2009). By applying N&B analysis to Cbl-inactivated HeLa cells, we now show that inhibition of FGFR1 degradation in FGF2-stimulated cells modifies the dynamics of FGFR1-mEGFP, resulting in the exposure of a long-lasting, promiscuous population of monomers and dimers at the cell surface. This behavior is highly reminiscent of the receptor transitions induced by NCAM.

Journal of Cell Science (2019) 132, jcs220624. doi:10.1242/jcs.220624

However, we have never observed the formation of larger FGFR1 clusters either after stimulation by low FGF2 concentrations or in dominant-negative Cbl cells that were stimulated with 20 ng/ml FGF2. We detected only oscillations between monomers and dimers. Given the profound difference between an Ig-like adhesion molecule, such as NCAM, and a polypeptide growth factor, such as FGF2, this might imply that the degree of FGFR1 clustering is not guided by the fate of the receptor itself but rather by the molecular nature of the stimulating ligand. Overall, our observations are consistent with the possibility that the different FGFR1-dependent cellular responses to FGF2 or NCAM depend, at least to some extent, on the mode of assembly and the dynamics of the receptor at the cell surface. Further investigation will be needed to identify the biological basis of the similar pattern of FGFR1 clustering and trafficking that is evoked by FGF2 in Cbl-inactivated cells, by low FGF2 concentrations and by NCAM.

We show here that the destabilization of FGFR1 dimers that are formed upon exposure to 20 ng/ml FGF2 occurred also after pre-treating the cells with filipin, which inhibits both raft- and caveolae-mediated endocytosis (Schnitzer et al., 1994). Also in this case, the cyclic dynamics and heterogeneity of receptor species at the cell surface might be ascribed to alterations of the endocytic trafficking of FGR1–FGF2 complexes. This result is consistent with the previous observations that disruption of lipid rafts causes reduced binding and increased dissociation rates of FGF2 from the cell surface, and decreased FGF2-mediated PKCα activation (Chu et al., 2004). By contrast, the inhibition of recycling by monensin altered the dynamics of FGFR1 only when the receptor was stimulated by NCAM-Fc, but had a negligible effect on FGFR1−FGF2 complexes. Thus, NCAM-dependent FGFR1 recycling is required for the correct assembly of NCAM–FGFR1 complexes at the cell surface.

Our observations are consistent with a model in which the clustering of FGFR1 complexes is orchestrated through the molecular nature of the ligand, while the stability of the complexes themselves depends on different factors – possibly including ligand affinity. Combining this paradigm with our previous results of the differential FGFR1 signaling elicited by NCAM and FGF2 (Francavilla et al., 2009), it is possible that differential clustering induced by different ligands accounts for distinct biochemical and cellular responses. Such a possibility points to the assembly and dynamics of the receptor complexes as a further level of intricacy in the regulation of FGFR1 function.

MATERIALS AND METHODS

Antibodies and reagents

The following antibodies were used: rabbit anti-GFP (1 µg/ml) produced by the Biochemistry Unit of the Consortium for Genomic Technologies (Cogentech; Milan, Italy); mouse anti-phosphotyrosine (1:200; BD Biosciences); rabbit anti-FGFR1 (C15; 1:200) and goat anti-actin (1:200; Santa Cruz Biotechnology, Inc); mouse anti-FGFR1 (M2F12; 1:200; Santa Cruz Biotechnology, Inc); mouse anti-phosphorylated-FGFR (55H2; 1:1000; Cell Signaling Technology). Secondary antibodies anti-rabbit, anti-mouse and anti-goat HRP linked were from Bio-Rad. The following reagents were used: recombinant FGF2 (Pepro Tech), recombinant NCAM-Fc produced as previously described (Francavilla et al., 2009), dendrimeric FGL peptide from the second FNIII module of NCAM (Kiselyov et al., 2003) (ENKAM Pharmaceuticals), monensin and filipin (Sigma-Aldrich).

Vectors

The cDNA encoding FGFR1 was provided by Jennifer Stow (Institute for Molecular Bioscience, University of Queensland, St. Lucia, Australia) (Bryant et al., 2005) and was subcloned into the expression vector for monomeric EGFP (pN1-mEGFP) generating FGFR1-mEGFP (Hellriegel et al., 2011).

Cell lines and transfection

HeLa cells were maintained in DMEM high-glucose GlutaMAX I medium (GIBCO) supplemented with 10% fetal bovine serum. Transfections were carried out using TransIt-LT1 reagent (MirusBio LLC) according to the manufacturer's instructions. HeLa cells stably transfected with dominant-negative Cbl (Penengo et al., 2006) were provided by Simona Polo (Milan, Italy). For microscopy, cells were plated and transfected in glass-bottom (glass thickness 0.16–0.19 mm) 35-mm dishes (MatTek). Cells were maintained in serum-free DMEM (0.1% BSA and 25 mM HEPES without Phenol Red) overnight before stimulation with 20, 10, 2 or 1 ng/ml FGF2, 50 µg/ml NCAM-Fc or 40 µg/ml FGL peptide. All ligands were diluted in PBS supplemented with 0.01%BSA, and the latter was used as vehicle control. All cell lines were regularly tested for mycoplasma contamination

Immunoblotting and immunoprecipitation

Cells were cultured in 6-well plates and transfected with FGFR1-mEGFP in complete medium. Twenty-four hours after transfection, cells were serum-starved overnight and then stimulated for the indicated time points with 50 µg/ml NCAM-Fc or 20 ng/ml FGF2. Cells were lysed in buffer containing 1% Triton X-100, 150 mM NaCl, 50 mM Tris-HCl (pH 7,6), 1 mM $CaCl_2$, 10 mM NaF, 1 mM sodium orthovanadate and protease inhibitors mix. Cell lysates were cleared by centrifugation at 14,000 ***g*** for 30 min. Proteins (25 µg/lane) were resolved by SDS-PAGE and transferred to nitrocellulose membranes (Protran, Whatman). Proteins of interest were visualized by using specific antibodies, followed by peroxidase-conjugated secondary antibodies. Chemiluminescent signals were detected using Clarity Western ECL Substrate (Bio-Rad). For immunoprecipitation, cell lysates were pre-cleared with non-immune IgG (Sigma-Aldrich) before incubation with anti-FGFR1 (C15), followed by addition of Protein A-Sepharose (Amersham-GE Healthcare). Immunoprecipitates were resolved by SDS–PAGE and analyzed by immunoblotting.

TIRF microscopy

FGFR1-mEGFP population on the ventral cell membrane was imaged by TIRF microscopy, taking advantage of the short penetration of evanescent illumination (Poulter et al., 2015) HeLa cells were serum-starved overnight and imaging started immediately after adding the ligands. Cells with exceedingly high fluorescence (i.e. overexpression of the ectopic construct) were excluded from the analysis. Cells were imaged by using a TIRF microscope (Leica AM, Wetzlar, Germany) equipped with an iXon897 EMCCD camera (Andor TM Technology, Belfast, North Ireland) and a thermostatic chamber to provide 5% CO_2 atmosphere and temperature at 37±0.5°C (Meyer Instruments, Houston, TX). For N&B, the camera was calibrated using the procedure previously described (Unruh and Gratton, 2008). Time stacks of images (700– 1000 frames, 256×256 pixels, 124 nm/pixels) were collected with a TIRF field of 110 nm, at 488 nm excitation and 1 ms/frame (22 ms accumulate cycle time). For N&B analysis, at least 500 frames were analyzed for each time stack using a customized MatLab routine (The MathWorks, Inc. Natick, MA) developed in house (Unit of Microscopy and Dynamic Imaging, CNIC, Madrid, Spain) and SimFCS software (Laboratory for Fluorescence Dynamics, Irvine, CA) after removing out-of focus frames.

N&B analysis

N&B is a pixel-by-pixel moment-analysis for measuring the average number of molecules (n) and brightness (ε) in each pixel, which are related to the average fluorescence intensity (<I>) as (Digman et al., 2008):

$$<I> = \varepsilon n \quad (1)$$

When the fluorophores in the sample are not too crowded (that is at low-moderate expression levels of fluorescence) the brightness (ε) of the fluorophore can be derived from the fluorescence fluctuation amplitudes caused by the fluorescent molecules diffusing in and out of the observation

volume by computing the ratio of the variance to the average intensity at each pixel (Dalal et al., 2008; Digman et al., 2008; Ossato et al., 2010; Unruh and Gratton, 2008). Thus, if a protein labeled with a fluorescent dye of brightness 1xε associates as a homodimer, the complex will carry 2 fluorescent labels, and the N&B analysis will yield a molecular brightness of 2xε. Mixed oligomer populations yield a mean brightness <ε> weighted by the fractional intensity (fi=Ii/ΣnIn) of the individual 'n' components: <ε>=Σn fn εn (Hellriegel et al., 2011).

After acquiring TIRF frames, images were averaged over time to compute the pixel-by-pixel averaged intensity (<I>) (Step 1 in Fig. 2). In step 2 (Fig. 2) the apparent pixel brightness (B) was obtained from the ratio between the variance and the average intensity at each pixel as $B=\sigma^2/<I>$. B versus values are illustrated by contour plots as B-histograms. The image above background that is selected for the analysis is indicated as Region of Interest (ROI). The brightness of each selected pixel of the ROI is computed as B-value and shown in the B-map (step 3 in Fig. 2). As described in (Ross et al., 2011) the analysis of the B-values distributions was used to determine the central value (±s.e.m.), representing the average apparent B-value of the image (step 4 in Fig. 2). The s.e.m. was calculated as the standard deviation among the brightness values of the independent pixels divided by the square root of the number of pixels. To construct a kinetic run, at least 6000 pixels (i.e. 6000 values of brightness) were analyzed in each single cell image per time point using GraphPad (GraphPad Software Inc., San Diego, CA). The average brightness, <ε>, expressed in [(counts/molecule)×dwell time], was then obtained from the equation:

$$\langle B\rangle = 1 + \langle \varepsilon\rangle \quad (2)$$

and data were normalized as:

$$\text{average brightness ratio} = \frac{\langle B_t\rangle - 1}{\langle B_0\rangle - 1} = \frac{\langle \varepsilon_t\rangle}{\langle \varepsilon_0\rangle} \quad (3)$$

Where $\langle B_t\rangle$ – is the average B-value measured at time t after ligand addition, $\langle B_0\rangle$is the average B-value measured at the time t=0 (5–10 s after ligand addition), which in all cases was in agreement with the value of the monomeric GPI-mEGFP control.

To build the kinetic run, a different cell was imaged in a different field of view at each time point to avoid photobleaching and photo-damaging due to repeated illumination. To avoid distortion of the brightness by intensity changes during acquisition, the total acquisition time was within 11–22 s and time series showing fluorescence intensity changes >5% were discarded (Fukushima et al., 2018; Hur et al., 2014; Trullo et al., 2013). Control time stacks were acquired in parallel for HeLa cells expressing GPI-mEGFP or GPI-mEGFP-mEGFP to account for the intrinsic variability of the laser power during each run.

A receptor state was arbitrarily defined as 'stable' when in the timeframe of three consecutive acquisition cycles (~4 min) the difference in average brightness between the three consecutive measurements remained within the standard deviation calculated on unstimulated cells [i.e. s.d.=±0.13 (counts/molecule)×dwell time)]. Otherwise, the receptor state was defined as 'unstable'.

Acknowledgements
The CNIC is supported by the Ministry of Ciencia, Innovaciòn y Universidades and the Pro CNIC Foundation, and is a Severo Ochoa Center of Excellence (SEV-2015-0505). We are grateful to ENKAM Pharmaceuticals, Jennifer Stow and Simona Polo, for providing reagents or cell lines, and to Stefano Freddi (Istituto Europeo di Oncologia, Milan) for assistance with confocal microscopy on OVCAR3 cells.

Competing interests
The authors declare no competing or financial interests.

Author contributions
Conceptualization: M.Z., U.C., V.R.C.; Methodology: M.Z., A.T.; Software: A.T.; Validation: M.Z.; Formal analysis: M.Z., A.T.; Investigation: M.Z., M.G., V.C., E.A.C.; Resources: C.F., U.C., V.R.C; Data curation: M.Z.; Writing - original draft: M.Z., M.G., V.R.C; Writing - review & editing: M.Z., M.G., U.C., V.R.C; Visualization: U.C., V.R.C; Supervision: U.C., V.R.C; Project administration: U.C., V.R.C; Funding acquisition: U.C., V.R.C.

Funding
U.C. and V.R.C. acknowledge the support of Fondazione CARIPLO, Milano (Grant 2375 2009-2012). U.C. also acknowledges the support from the Associazione Italiana Ricerca sul Cancro, the Association for International Cancer Research (now known as Worldwide Cancer Research), and the Italian Ministry of Health. A.T. acknowledges the 'Fondazione Banca del Monte di Lombardia' for partly supporting his work with the PV Fellowship 'Progetto Professionalitá Ivano Becchi' (2011-2012). M.G. was supported by a fellowship from Fondazione IEO-CCM.

Supplementary information
Supplementary information available online at
http://jcs.biologists.org/lookup/doi/10.1242/jcs.220624.supplemental

References
Anastasia, A., Barker, P. A., Chao, M. V. and Hempstead, B. L. (2015). Detection of p75NTR trimers: implications for receptor stoichiometry and activation. *J. Neurosci.* **35**, 11911-11920.
Asimaki, O., Leondaritis, G., Lois, G., Sakellaridis, N. and Mangoura, D. (2011). Cannabinoid 1 receptor-dependent transactivation of fibroblast growth factor receptor 1 emanates from lipid rafts and amplifies extracellular signal-regulated kinase 1/2 activation in embryonic cortical neurons. *J. Neurochem.* **116**, 866-873.
Babina, I. S. and Turner, N. C. (2017). Advances and challenges in targeting FGFR signalling in cancer. *Nat. Rev. Cancer* **17**, 318-332.
Balasubramanian, R. and Zhang, X. (2015). Mechanisms of FGF gradient formation during embryogenesis. *Semin. Cell Dev. Biol.* **53**, 94-100.
Basu, S. K., Goldstein, J. L., Anderson, R. G. W. and Brown, M. S. (1981). Monensin interrupts the recycling of low density lipoprotein receptors in human fibroblasts. *Cell* **24**, 493-502.
Beenken, A. and Mohammadi, M. (2009). The FGF family: biology, pathophysiology and therapy. *Nat. Rev. Drug Discov.* **8**, 235-253.
Belov, A. A. and Mohammadi, M. (2013). Molecular mechanisms of fibroblast growth factor signaling in physiology and pathology. *Cold Spring Harbor Perspect. Biol.* **5**.
Bryant, D. M., Wylie, F. G. and Stow, J. L. (2005). Regulation of endocytosis, nuclear translocation, and signaling of fibroblast growth factor receptor 1 by E-cadherin. *Mol. Biol. Cell* **16**, 14-23.
Caiolfa, V. R., Zamai, M., Malengo, G., Andolfo, A., Madsen, C. D., Sutin, J., Digman, M. A., Gratton, E., Blasi, F. and Sidenius, N. (2007). Monomer dimer dynamics and distribution of GPI-anchored uPAR are determined by cell surface protein assemblies. *J. Cell Biol.* **179**, 1067-1082.
Cavallaro, U., Niedermeyer, J., Fuxa, M. and Christofori, G. (2001). N-CAM modulates tumour-cell adhesion to matrix by inducing FGF-receptor signalling. *Nat. Cell Biol.* **3**, 650-657.
Chen, Y., Müller, J. D., Ruan, Q. Q. and Gratton, E. (2002). Molecular brightness characterization of EGFP in vivo by fluorescence fluctuation spectroscopy. *Biophys. J.* **82**, 133-144.
Christensen, C., Lauridsen, J. B., Berezin, V., Bock, E. and Kiselyov, V. V. (2006). The neural cell adhesion molecule binds to fibroblast growth factor receptor 2. *FEBS Lett.* **580**, 3386-3390.
Chu, C. L., Buczek-Thomas, J. A. and Nugent, M. A. (2004). Heparan sulphate proteoglycans modulate fibroblast growth factor-2 binding through a lipid raft-mediated mechanism. *Biochem. J.* **379**, 331-341.
Coffman, V. C. and Wu, J.-Q. (2012). Counting protein molecules using quantitative fluorescence microscopy. *Trends Biochem. Sci.* **37**, 499-506.
Dalal, R. B., Digman, M. A., Horwitz, A. F., Vetri, V. and Gratton, E. (2008). Determination of particle number and brightness using a laser scanning confocal microscope operating in the analog mode. *Microsc. Res. Tech.* **71**, 69-81.
Digman, M. A. and Gratton, E. (2011). Lessons in fluctuation correlation spectroscopy. *Annu. Rev. Phys. Chem.* **62**, 645-668.
Digman, M. A., Dalal, R., Horwitz, A. F. and Gratton, E. (2008). Mapping the number of molecules and brightness in the laser scanning microscope. *Biophys. J.* **94**, 2320-2332.
Eswarakumar, V. P., Lax, I. and Schlessinger, J. (2005). Cellular signaling by fibroblast growth factor receptors. *Cytokine Growth Factor. Rev.* **16**, 139-149.
Fecchi, K., Travaglione, S., Spadaro, F., Quattrini, A., Parolini, I., Piccaro, G., Raggi, C., Fabbri, A., Felicetti, F., Care, A. et al. (2012). Human melanoma cells express FGFR/Src/Rho signaling that entails an adhesion-independent caveolin-1 membrane association. *Int. J. Cancer.* **130**, 1273-1283.
Felder, S., Miller, K., Moehren, G., Ullrich, A., Schlessinger, J. and Hopkins, C. R. (1990). Kinase activity controls the sorting of the epidermal growth factor receptor within the multivesicular body. *Cell* **61**, 623-634.
Francavilla, C., Loeffler, S., Piccini, D., Kren, A., Christofori, G. and Cavallaro, U. (2007). Neural cell adhesion molecule regulates the cellular response to fibroblast growth factor. *J. Cell Sci.* **120**, 4388-4394.
Francavilla, C., Cattaneo, P., Berezin, V., Bock, E., Ami, D., de Marco, A., Christofori, G. and Cavallaro, U. (2009). The binding of NCAM to FGFR1 induces a specific cellular response mediated by receptor trafficking. *J. Cell Biol.* **187**, 1101-1116.

Fukushima, R., Yamamoto, J., Ishikawa, H. and Kinjo, M. (2018). Two-detector number and brightness analysis reveals spatio-temporal oligomerization of proteins in living cells. *Methods* **140-141**, 161-171.
Furdui, C. M., Lew, E. D., Schlessinger, J. and Anderson, K. S. (2006). Autophosphorylation of FGFR1 kinase is mediated by a sequential and precisely ordered reaction. *Mol. Cell* **21**, 711-717.
Garcia-Maya, M., Anderson, A. A., Kendal, C. E., Kenny, A. V., Edwards-Ingram, L. C., Holladay, A. and Saffell, J. L. (2006). Ligand concentration is a driver of divergent signaling and pleiotropic cellular responses to FGF. *J. Cell. Physiol.* **206**, 386-393.
Germano, S., Barberis, D., Santoro, M. M., Penengo, L., Citri, A., Yarden, Y. and Gaudino, G. (2006). Geldanamycins trigger a novel Ron degradative pathway, hampering oncogenic signaling. *J. Biol. Chem.* **281**, 21710-21719.
Gleizes, P. E., Noaillac-Depeyre, J., Dupont, M. A. and Gas, N. (1996). Basic fibroblast growth factor (FGF-2) is addressed to caveolae after binding to the plasma membrane of BHK cells. *Eur. J. Cell Biol.* **71**, 144-153.
Hansen, S. M., Kohler, L. B., Li, S., Kiselyov, V., Christensen, C., Owczarek, S., Bock, E. and Berezin, V. (2008). NCAM-derived peptides function as agonists for the fibroblast growth factor receptor. *J. Neurochem.* **106**, 2030-2041.
Hellriegel, C., Caiolfa, V. R., Corti, V., Sidenius, N. and Zamai, M. (2011). Number and brightness image analysis reveals ATF-induced dimerization kinetics of uPAR in the cell membrane. *FASEB J.* **25**, 2883-2897.
Hur, K.-H., Macdonald, P. J., Berk, S., Angert, C. I., Chen, Y. and Mueller, J. D. (2014). Quantitative measurement of brightness from living cells in the presence of photodepletion. *PLoS ONE* **9**, e97440.
Irschick, R., Trost, T., Karp, G., Hausott, B., Auer, M., Claus, P. and Klimaschewski, L. (2013). Sorting of the FGF receptor 1 in a human glioma cell line. *Histochem. Cell Biol.* **139**, 135-148.
Kanodia, J., Chai, D., Vollmer, J., Kim, J., Raue, A., Finn, G. and Schoeberl, B. (2014). Deciphering the mechanism behind Fibroblast Growth Factor (FGF) induced biphasic signal-response profiles. *Cell Commun. Signal.* **12**, 34.
Kiselyov, V. V., Skladchikova, G., Hinsby, A. M., Jensen, P. H., Kulahin, N., Soroka, V., Pedersen, N., Tsetlin, V., Poulsen, F. M., Berezin, V. et al. (2003). Structural basis for a direct interaction between FGFR1 and NCAM and evidence for a regulatory role of ATP. *Structure* **11**, 691-701.
Kos, F. J. and Chin, C. S. (2002). Costimulation of T cell receptor-triggered IL-2 production by Jurkat T cells via fibroblast growth factor receptor 1 upon its engagement by CD56. *Immunol. Cell Biol.* **80**, 364-369.
Lajoie, P. and Nabi, I. R. (2007). Regulation of raft-dependent endocytosis. *J. Cell. Mol. Med.* **11**, 644-653.
Lehembre, F., Yilmaz, M., Wicki, A., Schomber, T., Strittmatter, K., Ziegler, D., Kren, A., Went, P., Derksen, P. W., Berns, A. et al. (2008). NCAM-induced focal adhesion assembly: a functional switch upon loss of E-cadherin. *EMBO J.* **27**, 2603-2615.
Mohammadi, M., Olsen, S. K. and Ibrahimi, O. A. (2005). Structural basis for fibroblast growth factor receptor activation. *Cytokine Growth Factor. Rev.* **16**, 107-137.
Müller, J. D. (2004). Cumulant analysis in fluorescence fluctuation spectroscopy. *Biophys. J.* **86**, 3981-3992.
Nagy, P., Claus, J., Jovin, T. M. and Arndt-Jovin, D. J. (2010). Distribution of resting and ligand-bound ErbB1 and ErbB2 receptor tyrosine kinases in living cells using number and brightness analysis. *Proc. Natl. Acad. Sci. USA* **107**, 16524-16529.
Olivera-Couto, A., Salzman, V., Mailhos, M., Digman, M. A., Gratton, E. and Aguilar, P. S. (2015). Eisosomes are dynamic plasma membrane domains showing pil1-lsp1 heteroligomer binding equilibrium. *Biophys. J.* **108**, 1633-1644.
Ossato, G., Digman, M. A., Aiken, C., Lukacsovich, T., Marsh, J. L. and Gratton, E. (2010). A two-step path to inclusion formation of huntingtin peptides revealed by number and brightness analysis. *Biophys. J.* **98**, 3078-3085.
Perumal, V., Krishnan, K., Gratton, E., Dharmarajan, A. M. and Fox, S. A. (2015). Number and brightness analysis of sFRP4 domains in live cells demonstrates vesicle association signal of the NLD domain and dynamic intracellular responses to Wnt3a. *Int. J. Biochem. Cell Biol.* **64**, 91-96.
Plotegher, N., Gratton, E. and Bubacco, L. (2014). Number and Brightness analysis of alpha-synuclein oligomerization and the associated mitochondrial morphology alterations in live cells. *Biochim. Biophys. Acta* **1840**, 2014-2024.
Penengo, L., Mapelli, M., Murachelli, A. G., Confalonieri, S., Magri, L., Musacchio, A., Di Fiore, P. P., Polo, S., Schneider, T.R. (2006). Crystal structure of the ubiquitin binding domains of rabex-5 reveals two modes of interaction with ubiquitin. *Cell* **124**, 1183-1195.
Poulter, N. S., Pitkeathly, W. T. E., Smith, P. J. and Rappoport, J. Z. (2015). The physical basis of total internal reflection fluorescence (TIRF) microscopy and its cellular applications. *Methods Mol. Biol.* **1251**, 1-23.
Ridyard, M. S. and Robbins, S. M. (2003). Fibroblast growth factor-2-induced signaling through lipid raft-associated fibroblast growth factor receptor substrate 2 (FRS2). *J. Biol. Chem.* **278**, 13803-13809.
Ross, J. A., Digman, M. A., Wang, L., Gratton, E., Albanesi, J. P. and Jameson, D. M. (2011). Oligomerization state of dynamin 2 in cell membranes using TIRF and number and brightness analysis. *Biophys. J.* **100**, L15-L17.
Sanchez-Heras, E., Howell, F. V., Williams, G. and Doherty, P. (2006). The fibroblast growth factor receptor acid box is essential for interactions with N-cadherin and all of the major isoforms of neural cell adhesion molecule. *J. Biol. Chem.* **281**, 35208-35216.
Schnitzer, J. E., Oh, P., Pinney, E. and Allard, J. (1994). Filipin-sensitive caveolae-mediated transport in endothelium: reduced transcytosis, scavenger endocytosis, and capillary permeability of select macromolecules. *J. Cell Biol.* **127**, 1217-1232.
Sedger, L. M. and McDermott, M. F. (2014). TNF and TNF-receptors: From mediators of cell death and inflammation to therapeutic giants-past, present and future. *Cytokine Growth Factor. Rev.* **25**, 453-472.
Thomaidou, D., Coquillat, D., Meintanis, S., Noda, M., Rougon, G. and Matsas, R. (2001). Soluble forms of NCAM and F3 neuronal cell adhesion molecules promote Schwann cell migration: identification of protein tyrosine phosphatases zeta/beta as the putative F3 receptors on Schwann cells. *J. Neurochem.* **78**, 767-778.
Trullo, A., Corti, V., Arza, E., Caiolfa, V. R. and Zamai, M. (2013). Application limits and data correction in number of molecules and brightness analysis. *Microsc. Res. Tech.* **76**, 1135-1146.
Unruh, J. R. and Gratton, E. (2008). Analysis of molecular concentration and brightness from fluorescence fluctuation data with an electron multiplied CCD camera. *Biophys. J.* **95**, 5385-5398.
Wiedlocha, A. and Sorensen, V. (2004). Signaling, internalization, and intracellular activity of fibroblast growth factor. *Curr. Top. Microbiol. Immunol.* **286**, 45-79.
Williams, E. J., Furness, J., Walsh, F. S. and Doherty, P. (1994). Activation of the FGF receptor underlies neurite outgrowth stimulated by L1, N-CAM, and N-cadherin. *Neuron* **13**, 583-594.
Wong, E. S. M., Fong, C. W., Lim, J., Yusoff, P., Low, B. C., Langdon, W. Y. and Guy, G. R. (2002). Sprouty2 attenuates epidermal growth factor receptor ubiquitylation and endocytosis, and consequently enhances Ras/ERK signalling. *EMBO J.* **21**, 4796-4808.
Zecchini, S., Bombardelli, L., Decio, A., Bianchi, M., Mazzarol, G., Sanguineti, F., Aletti, G., Maddaluno, L., Berezin, V., Bock, E. et al. (2011). The adhesion molecule NCAM promotes ovarian cancer progression via FGFR signalling. *EMBO Mol. Med.* **3**, 480-494.

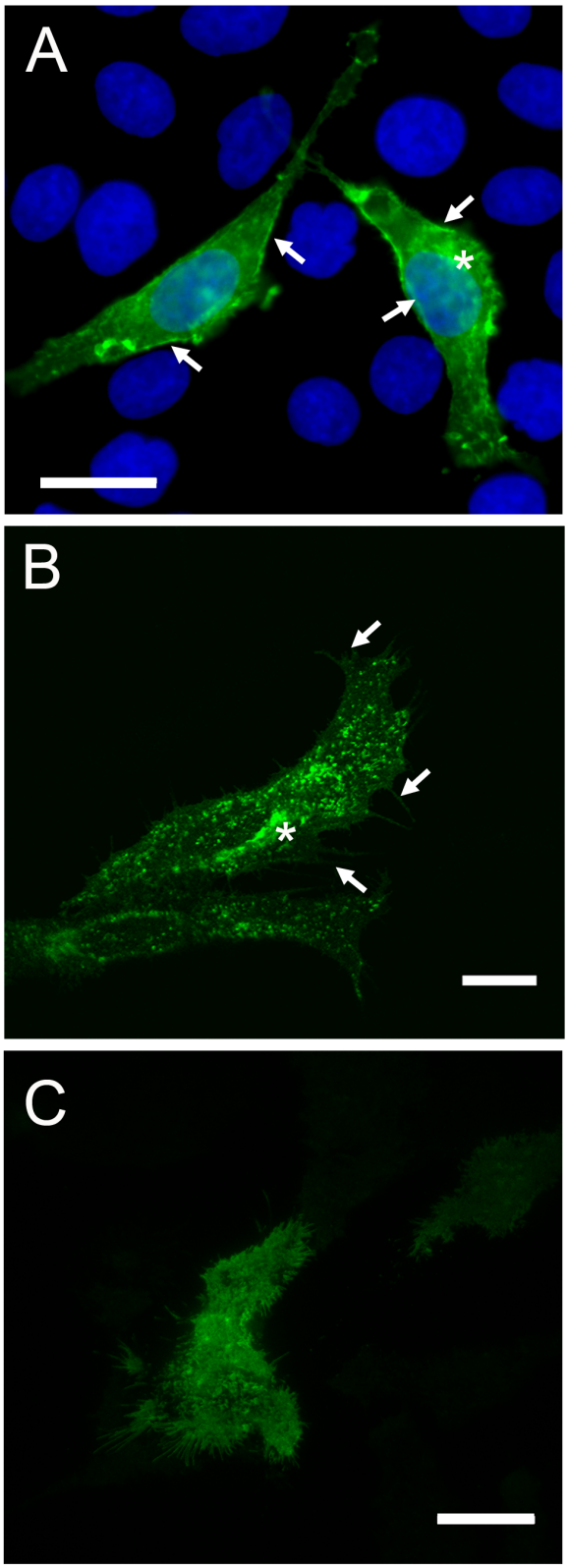

Figure S1 - Cellular distribution and localization of FGFR1-mEGFP transfected in HeLa cells grown to sub-confluence as it can be visualized by epifluorescence, confocal and TIRF microscopy.

Representative samples were imaged by:
(A) Epifluorescence microscopy. Cells were fixed and stained post-fixation with DAPI to mark the nuclei. Scale bar 20 µm.
(B) Confocal microscopy. Live cells were maintained in the culture medium, at 37 °C and 5%CO_2. The intracellular distribution of the receptor is visualized with a single optical section within a z-depth resolution of 1 µm at excitation of 488 nm. Scale bar 10 µm.
(C) TIRF microscopy. Live cells were maintained in the culture medium, at 37 °C and 5%CO_2. The distribution of the receptor is visualized under an evanescent field depth of <110 nm from the cover slide support. The image reproduces the acquisition conditions used for the N&B analysis. Scale bar 20 µm.

The receptor is found in the Golgi membranes (asterisks) and in the plasma membrane and filopodia (arrows). FGFR1-mEGFP is also recognized in vesicular structures. Based on the intrinsic features of evanescent illumination, the TIRF image depicts the ventral side of the plasma membrane, without interference coming from intracellular fluorescence signals. Under these conditions, FGFR1-mEGFP is clearly and abundantly localized on the ventral cell surface.

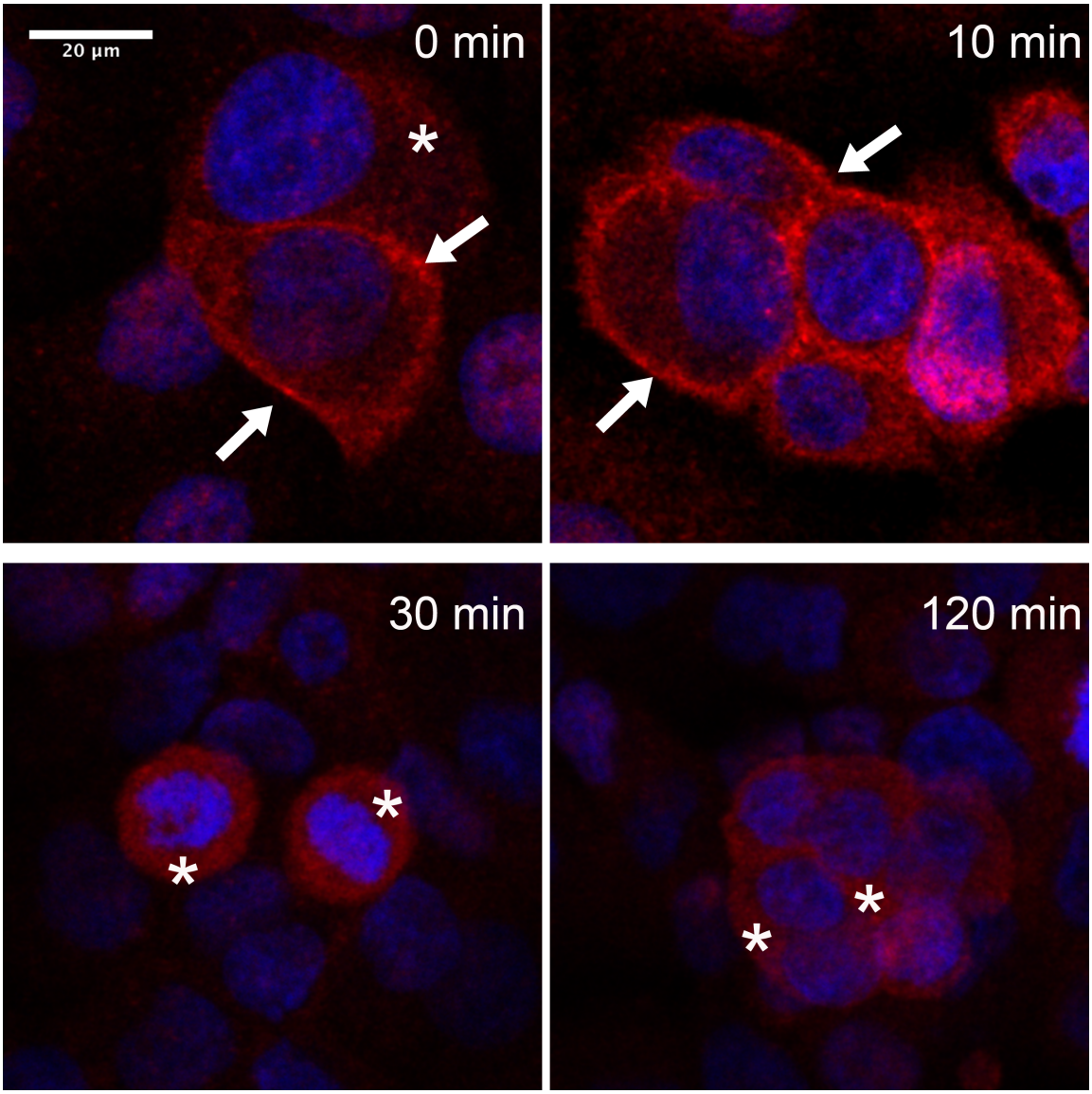

Figure S2 - Immunostaining of endogenous FGFR1 in OVCAR3 cells.

The human ovarian cancer cell line OVCAR3 was serum-starved over-night and treated for the indicated time with 20 ng/ml of FGF2. Cells were then fixed in 4% paraformaldehyde and permeabilized with ice-cold PBS and 0.5% Triton X-100 for 3 minutes on ice. Endogenous FGFR1 was predominantly localized at the plasma membrane in untreated cells and in cells stimulated with FGF2 (20 ng/ml) for 10 minutes (arrows), although some cytoplasmic localization could also be detected (asterisks). At longer incubation times, cells exhibited intracellular localization of the receptor, consistent with FGF2-induced internalization of FGFR1. The decreased intensity of the staining at 2 hours is likely due to the degradation of internalized receptor. Nuclei are stained with DAPI, FGFR1 visualized with FGFR1 antibody (clone M2F12) followed by a Donkey anti-mouse Cy-3 secondary antibody. Scale bar 20 µm.

Figure S1

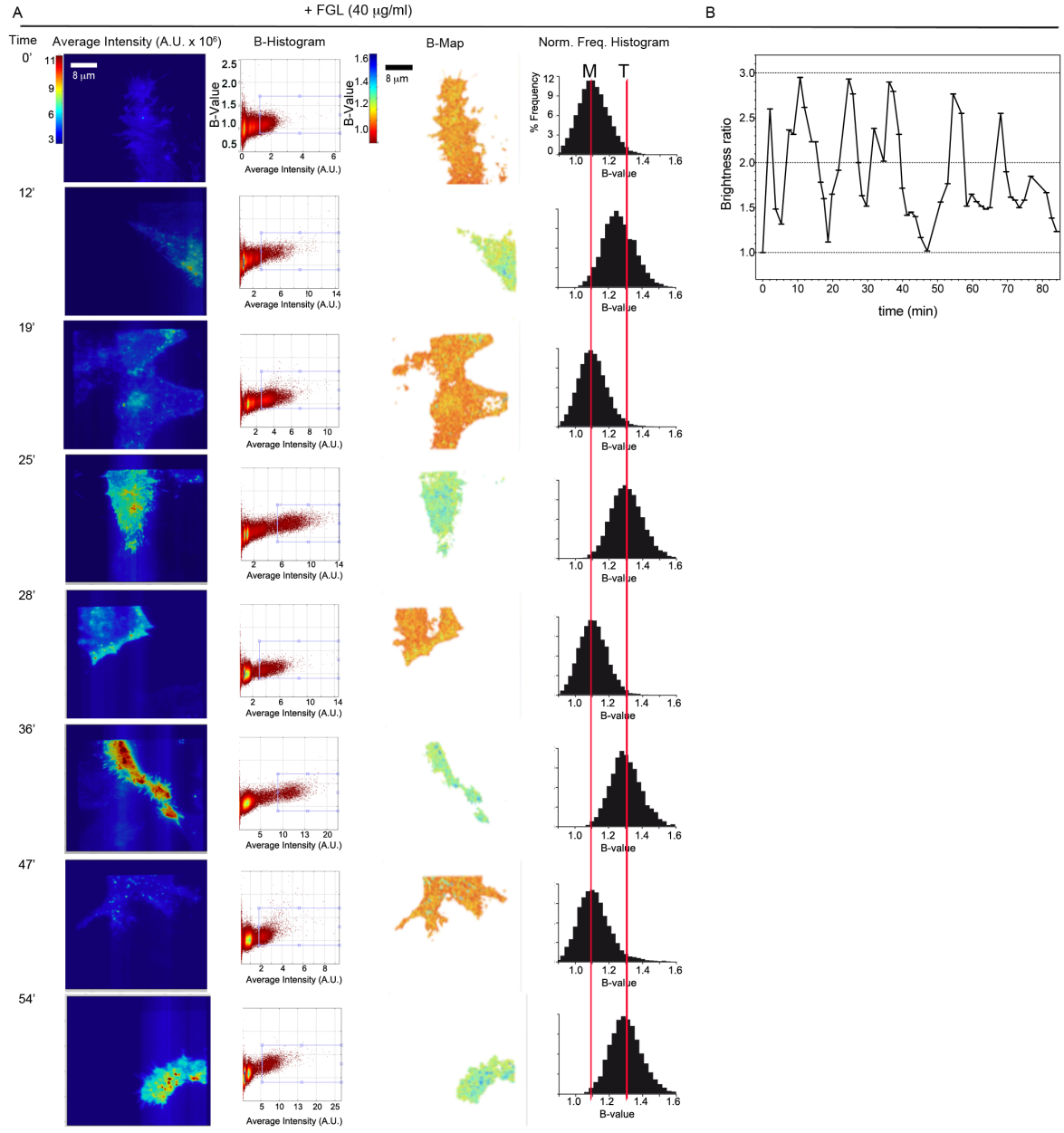

Figure S3. N&B analysis on cells stimulated with the FGL peptide.

(A) Representative example of a N&B kinetic of FGFR1-mEGFP expressed in Hela cells upon stimulation with FGL dendrimer peptide at 40 μg/ml. TIRF images series were collected and analyzed as described for Figure 2. The red lines in the Frequency Histograms (Norm. Freq. Histogram) mark the B-central values (average brightness) associated to mEGFP single unit (M = 1 unit) and mEGFP putative trimers (T= 3 units), as an indication of the shift observed during the kinetic runs. (B) Plot of average brightness as a function of time. Each value (± s.e.m.) was obtained as described in figure 3 (n=53 cells).

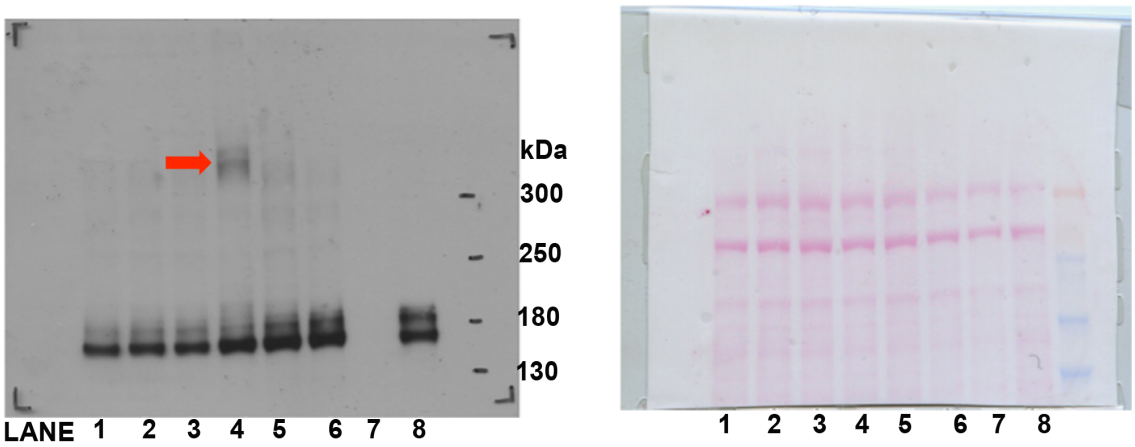

Lane 1: FGL 50 µg/ml, (7.14 µM) 2h, 4°C
Lane 2: NCAM-Fc 50 µg/ml, (192 nM) 2h, 4°C
Lane 3: NCAM-Fc 100 µg/ml, (384 nM) 2h, 4°C
Lane 4: FGF2, 20 ng/ml (1.16 nM) 30 min, 4°C
Lane 5: No Ligand + crosslinker
Lane 6: No Ligand - crosslinker
Lane 7: empty vector + crosslinker
Lane 8: replicate no ligand - crosslinker

Figure S4 Cross-linking of stimulated FGFR1-mEGFP.

HeLa cells transfected with FGFR1-mEGFP were incubated at 4°C with NCAM-Fc or FGF2 at the indicated concentrations and time lengths. Cell-surface proteins were then cross-linked with 2 mM BS^3. Cells were lysed and proteins were resolved by SDS-PAGE and transferred to nitrocellulose membranes; equal loading was confirmed by Ponceau S staining (right panel). FGFR1-mEGFP was visualized using rabbit anti-GFP (left panel). The arrow indicates the band corresponding to the FGFR1-mEGFP dimer.

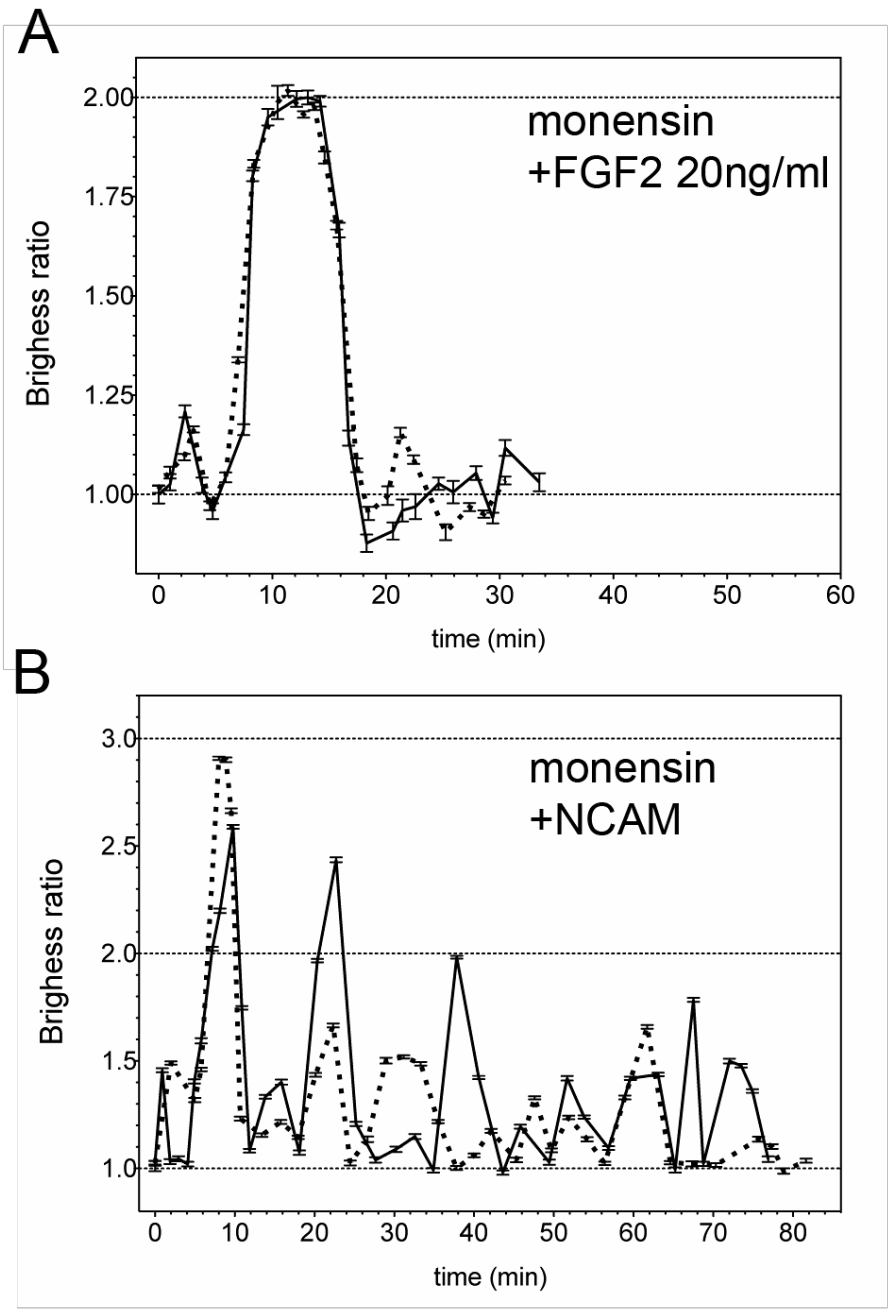

Figure S5. Inhibition of recycling alters the FGFR1 complex assembly in response to NCAM.

HeLa cells transfected with FGFR1-mEGFP were pre-treated with 50 mM monensin and stimulated with 20 ng/ml FGF2 (A) or 50 mg/ml NCAM-Fc (B). N&B kinetics were acquired as described in Figure 2 and 3. Cells: 23 (·····), 24 (——) in panel A, 38 (·····), 38 (——) in panel B. Data are provided as normalized brightness ratio (± s.e.m.) according to eq. (3) as described in figure 3.